Electron microprobe monazite geochronology : a tool for evaluating magmatic ages with examples from Variscan Massif Central migmatites and granotoids, France.

Eugène Be Mezeme, Alain Cocherie, Michel Faure, O. Lengendre, Philippe Rossi

Electron microprobe monazite geochronology of magmatic events: Examples from Variscan migmatites and granitoids, Massif Central, France

E. Be Mezeme[a, b], A. Cocherie[a], M. Faure[b], O. Legendre[a] and Ph. Rossi[a]

[a]BRGM-3, avenue Claude Guillemin, BP 6009, 45060 Orléans, France
[b]ISTO bâtiment Géosciences, BP 6759, 45067 Orléans Cedex 2, France

Abstract

U–Th–Pb dating of monazite with the electron probe microanalyser (EPMA) is increasingly documented as a reliable geochronological method offering high spatial resolution. This method has been applied on monazite from the Cévennes migmatites and granitoids from the southeast of the French Massif Central. Measurements were performed on separated grains after systematic back-scattered electron (BSE) imaging. Monazites from migmatites record two main ages: (i) a protolith age of about 550–543 Ma obtained on inherited cores, and (ii) a migmatization event between 329 ± 5 and 323 ± 3 Ma recorded by monazite rims and all other monogenetic grains. Monazite from the peraluminous Rocles pluton yields a 318 ± 3 Ma age. Finally, three granite dykes are dated at 333 ± 6, 318 ± 5 and 311 ± 5 Ma; the older dyke is the most deformed of them and is interpreted as linked to the migmatization event; the two other dykes are geochronologically, petrologically and structurally coeval with the Rocles pluton. The data constrain the timing of crustal melting following Variscan thickening in the northern Cévennes area. Migmatization of Ordovician protoliths took place at 329–323 Ma and was shortly followed by intrusion of leucogranite at 318–311 Ma. The study shows that EPMA dating of monazite can be successfully used to resolve a close succession of regional melting events.

Keywords: Monazite; Electron microprobe; Geochronology; Massif Central, France

1. Introduction

Monazite is a suitable chronometer for studying magmatic and polymetamorphic events due to its high Th and U contents and negligible common Pb content (Parrish, 1990). U–Th–Pb dating of monazite with the electron microprobe microanalyser (EPMA) has been recently developed into an alternative, accurate, and truly in situ means of geochronology, providing valuable constraints on the timing of metamorphic assemblages at a μm scale (Williams and Jercinovic, 2002). This new approach shed new light on the U–Th–Pb systematics in this mineral. It has thrown several earlier beliefs into question by showing that: the closure temperature of the system is significantly higher than 900 °C (Braun et al., 1998); inheritance in monazite is rather common as shown by Cocherie et al., 1998 and Cocherie et al., 2005; if no fluid interacts with monazite (Townsend et al., 2000), Pb diffusion is negligible (Cocherie et al., 1998, Crowley and Ghent, 1999 and Zhu and O'Nions, 1999).

In the present study, we dated specific monazite crystals from migmatites, granitic plutons and dykes in the Cévennes area of the French Massif Central. The main geological questions

concern the genetic relationships between the migmatites, the Rocles pluton and leucogranite dykes. The occurrence within a relatively small area of several generations of plutonic and migmatitic rocks, probably formed during a short time span, provided an ideal opportunity for using the EPMA monazite dating method, in order to distinguish the succession of melting events, and to assess the ability of the method to establish the ages of the protoliths. As shown in the following sections, EPMA U–Th–Pb dating on monazite suggests distinct timing for migmatization and leucogranite plutonism.

2. Geological setting

The analysed samples come from the Cévennes area in the southeastern part of the Variscan French Massif Central (Fig. 1, with sample locations). A continental collision between two large continental masses, Gondwana and Baltica, and several intervening microcontinents marked the pre-Permian tectonic evolution of France. In the southern Massif Central, top-to-the-south ductile shearing caused nappe stacking (e.g., Ledru et al., 1989 and Faure et al., 1997; and references therein). After the continental collision, the Variscan belt underwent major crustal melting from Late Devonian to Late Carboniferous times, at the expense of metapelites and metagranites (e.g., Duthou et al., 1984 and Pin and Duthou, 1990).

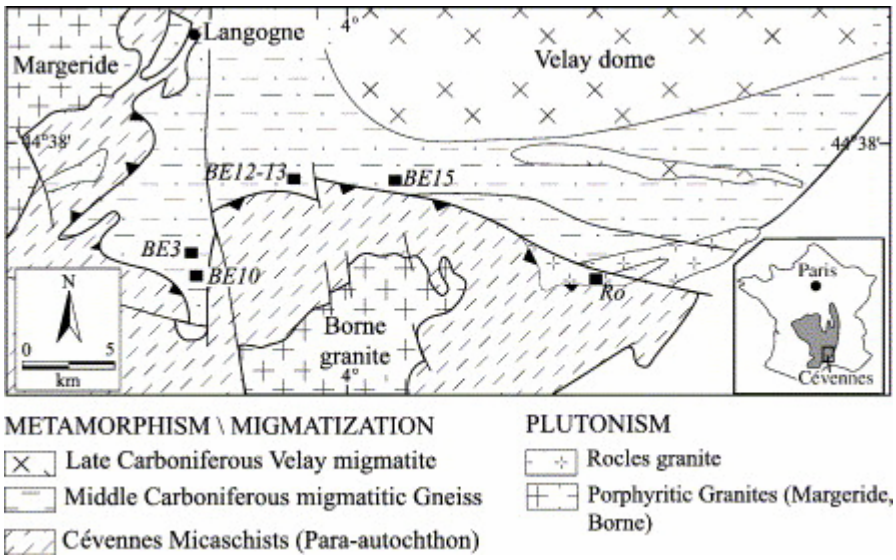

Fig. 1. Structural map of the North Cévennes area with the location of investigated samples (dark squares). Insert locates the study area in the French Massif Central.

The Cévennes area is a circa 5-km-thick stack of thrust sheets with metapelite, metagraywacke and quartzite belonging to the Parautochtonous Unit that was transported southward over an underlying augen orthogneiss and biotite–muscovite paragneiss units (Faure et al., 2001). South of the study area, synmetamorphic shearing was dated around 340–335 Ma by ^{40}Ar / ^{39}Ar method on micas and amphiboles (Caron, 1994; see review in Faure et al., 2001).

Thrusting was followed by crustal melting producing biotite–sillimanite migmatite and granite that are well exposed south of Langogne and are called locally the "Puylaurent migmatite" (Fig. 1 and Fig. 2a). Field relationships show that anatexis developed at the expense of augen orthogneiss under thermo-barometric conditions estimated at $T < 750$ °C

and $P > 5$ kbar (Montel et al., 1992). Several granite intrusions intersect the Cévennes metamorphic rocks, the most important being a porphyritic monzogranite that, in the study area, corresponds to the Margeride and the Borne massifs (Fig. 1). Rb–Sr whole-rock dating of this granite gave an age of 315 ± 5 Ma (Mialhe, 1980). Recent U–Pb dating on zircon from an eastern biotite-rich facies of the Margeride pluton gave 311 ± 6 Ma (Isnard, 1996). Peraluminous two-mica leucogranite forms small plutons, such as the Rocles massif, and metre-scale dykes intruding the Puylaurent migmatite, Cévennes micaschist and Borne granite. Rb–Sr whole-rock dating of the Rocles granite gave an age of 302 ± 4 Ma age (Caen-Vachette et al., 1981). Leucogranite dykes are widespread near the thrust fault between the Cévennes mica-schist and the Puylaurent migmatite. Immediately north of the study area, Late Carboniferous cordierite granite and migmatite form the Velay dome.

3. Sample description

3.1. Migmatite

Two samples (BE3 and BE13) were collected from the Puylaurent migmatite (Table 1, Fig. 1 and Fig. 2a). Field observations show that the migmatite developed at the expense of augen orthogneiss. By analogy with the southern Cévennes area, it is likely that the ductile synmetamorphic deformation, which produced the orthogneiss, occurred around 340–335 Ma. The age of the granitic protolith is presently unknown, but in other places of the French Massif Central such orthogneisses yield Cambrian or Ordovician ages (e.g., Duthou et al., 1984 and Pin and Duthou, 1990). Under the microscope, the leucosome consists of quartz and K-feldspar recrystallized under high-temperature conditions (Fig. 2b). Most of the biotite is located in the melanosome; biotite crystals contain a large number of inclusions of zircon, monazite (Fig. 2c), apatite and euhedral pyrite. In addition to this primary magmatic assemblage, secondary minerals such as muscovite, chlorite and Fe-oxides, partly related to late fluid circulation, occur.

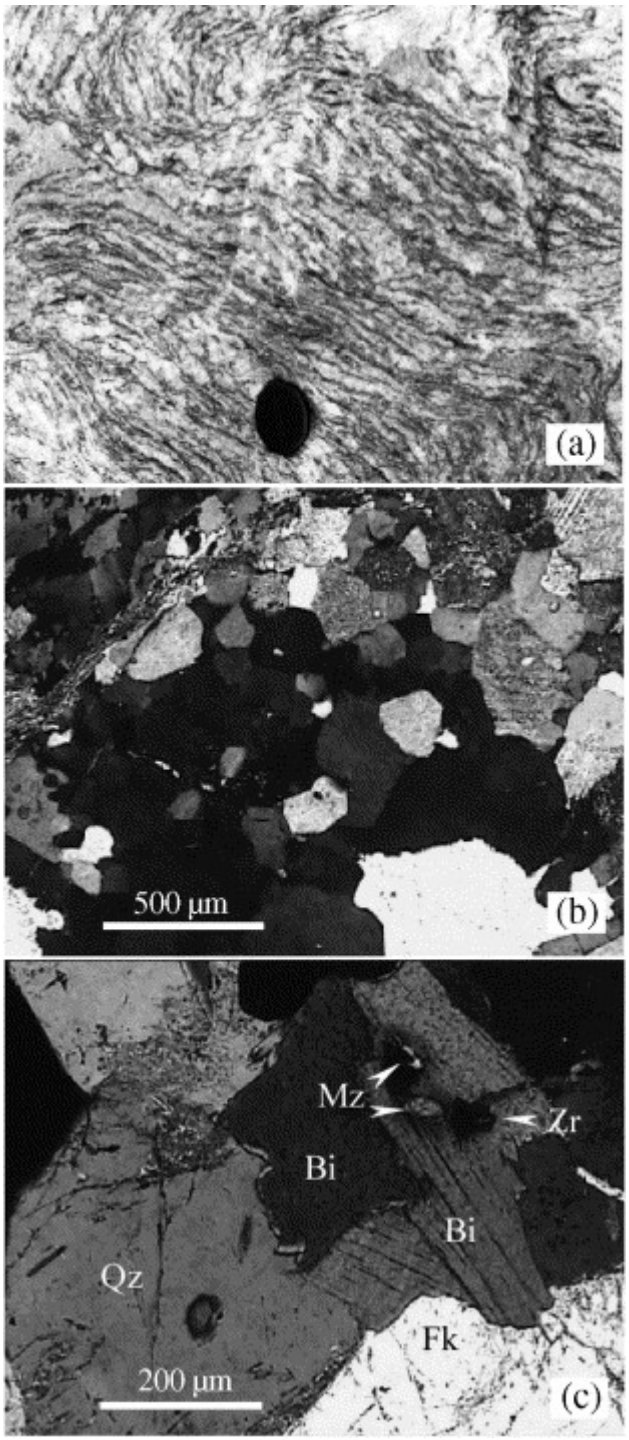

Fig. 2. (a) Outcrop-scale picture of Puylaurent migmatite: dark-coloured layers are biotite-rich. The protolith was an augen gneiss. (b) Thin section showing typical fabric of statically recrystallized quartz and feldspar with triple point. (c) Monazite and zircon inclusions in biotite from sample BE13.

Table 1. : Summary of electron microprobe data for analyzed monazites showing the range of U, Th and Pb variation for each sample

Pb (ppm) ± σ	**U (ppm) ± σ**	**Th (ppm) ± σ**	**Th / U ± σ**	**Isochron age ± 2σ Ma**	**No. of data**
Puylaurent migmatite BE3 (03°54′22″–44°35′36″)					
Eight monazite grains (without grain 12)					
1890 ± 436	19,645 ± 8865	68,193 ± 21,409	6.2 ± 7.6	323 ± 3	99
Rim of complex monazite Grain 12					
1912 ± 403	19,777 ± 9337	68,892 ± 11,531	7.2 ± 9.0	324 ± 6	38
Core of complex monazite Grain 12					
1264 ± 169	1152 ± 313	46,227 ± 4622	42 ± 9	550 ± 86	34
Puylaurent migmatite BE13 (03°58′14″–44°36′26″)					
Six monazite grains (without grain 3)					
1306 ± 153	13,602 ± 3013	48,424 ± 4021	3.7 ± 0.8	322 ± 7	55
Rim of complex monazite Grain 3					
1507 ± 167	14,922 ± 2868	55,782 ± 4057	4.0 ± 1.7	329 ± 5	111
Core of complex monazite Grain 3					
1965 ± 578	4750 ± 4181	65,313 ± 10,953	20 ± 8	543 ± 25	8
Rocles granite Ro, four monazite grains (04°11′20″–44°32′47″)					
2810 ± 569	42,227 ± 18,248	62,128 ± 22,317	2.1 ± 1.9	318 ± 3	36
Leucogranite dyke BE10, ten monazite grains (03°54′37″–44°31′20″)					
1143 ± 300	8278 ± 6310	51,834 ± 11,996	10.8 ± 10.2	333 ± 6	69
Leucogranite dyke BE12, two monazite grains (03°58′14″–44°36′26″)					
1601 ± 643	19,866 ± 9474	49,933 ± 18,054	3.2 ± 2.8	318 ± 5	32
Leucogranite dyke BE15 (04°03′58″–44°36′46″)					
Nine monazite grains (without grain 5)					
2336 ± 612	39,582 ± 12,481	41,508 ± 7442	1.2 ± 0.4	311 ± 5	85

Pb (ppm) ± σ	U (ppm) ± σ	Th (ppm) ± σ	Th / U ± σ	Isochron age ± 2σ Ma	No. of data
Rim of complex monazite Grain 5					
2998 ± 447	50,210 ± 10,529	56,383 ± 10,485	1.3 ± 0.8	309 ± 4	43
Core of complex monazite Grain 5					
2343 ± 549	4026 ± 826	140,846 ± 33,072	35 ± 5	341 ± 14	85

Note that for polygenetic grains, the average values are calculated according to domains that are homogeneous in age.

3.2. Rocles granite and leucogranitic dykes

Four leucogranitic rocks were sampled (Table 1, Fig. 1). The Rocles pluton (Ro sample) is exposed in the easternmost part of the study area (Fig. 1); it is a peraluminous granite emplaced along the tectonic contact between the parautochtonous micaschist and the underlying migmatized gneiss (Palm, 1957 and Weisbrod, 1968). Three lithological units, distinguished on the basis of their mineralogy, crop out from north to south, that is to say from bottom to top of the pluton: i) a porphyritic biotite-rich, muscovite-free facies forms the northern part of the pluton, where cm-to m-sized xenoliths of country rock are widespread; ii) a muscovite–biotite leucogranite with some euhedral garnet is exposed in the central part of the pluton; iii) a biotite-free, muscovite-rich granite is the structurally highest and southernmost facies. Under the microscope, quartz displays wavy extinction and locally dynamic recrystallization characterized by small neograins with serrated boundaries. Feldspar is commonly cataclased and mica crystals commonly show a preferred orientation. These textural observations suggest that the Rocles granite experienced a magmatic to sub-solidus deformation coeval with its emplacement.

Samples BE10, BE12 and BE15 were taken from granite veins intruding migmatite or gneiss (Fig. 3a); some of those veins are boudinaged and have a sigmoidal shape with top-to-the-N sense of shear (Fig. 3b). Microscopically, the veins have a common granite mineralogy, namely quartz, K-feldspar, biotite and muscovite. Zircon, monazite and apatite are common accessory phases. Although the veins have a weak fabric at the hand-specimen scale, micas exhibit under the microscope a clear shape-preferred orientation. Dynamic recrystallization has developed in magmatic quartz grains, and feldspars are commonly cataclased. It is worth noting that sample BE10 appears more deformed (Fig. 3c) than samples BE12 and BE15.

4. Analytical method

Monazite grains were separated, mounted in resin and polished to obtain cross-sections and analysed with a Cameca SX 50 electron microprobe; for the detailed analytical procedure see Cocherie et al. (1998). According to this procedure, detection limit (2σ) is 150 ppm for Pb and U, the absolute error being taken as 150 ppm.

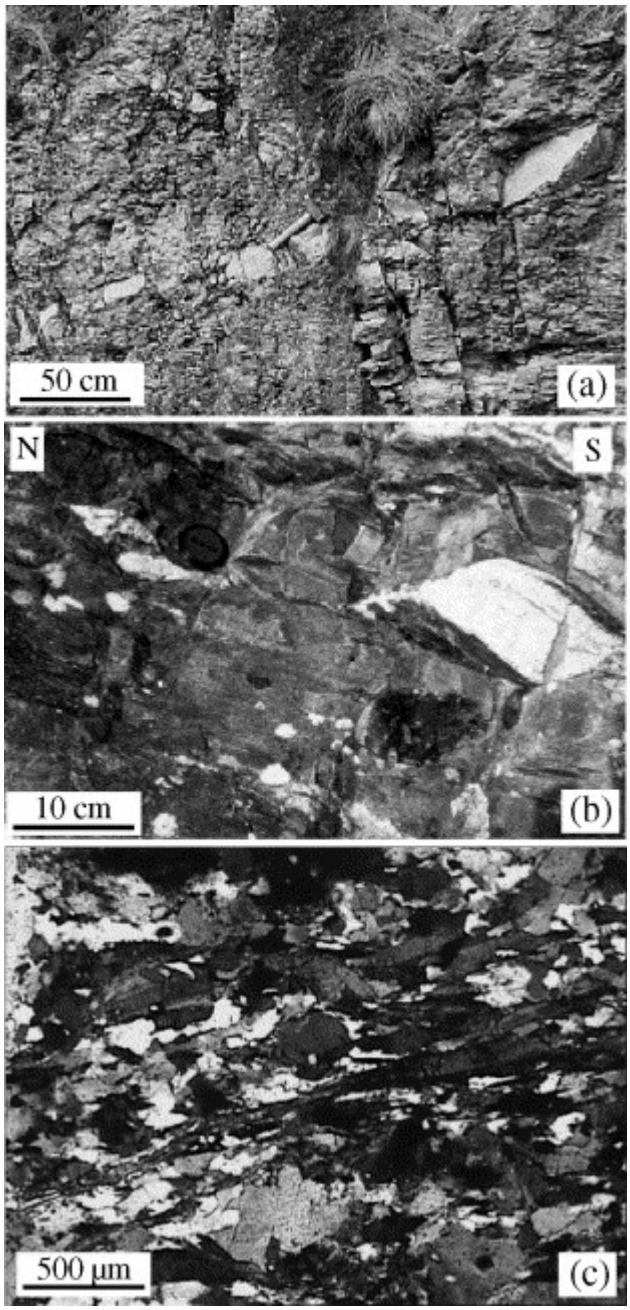

Fig. 3. (a) Example of granite dykes that transect the migmatitic augen gneiss. (b) Dykes are boudinaged with sigmoidal shape showing top-to-the north shearing. (c) Thin section from leucogranite vein BE10 showing intense dynamic recrystallization of quartz.

A systematic relative error of 2% is considered for Th as well as for U concentrations above 7500 ppm, in order to avoid an unrealistic low error for U-enriched grains. In obvious need of a program to simplify the individual age and isochron mean age calculations, Pommier et al. (2002) wrote *EPMA Dating*, a Microsoft Excel add-in program for determining U–Th–Pb_{tot} ages from electron probe microanalyser (EPMA) measurements. This program calculates an age for each individual point analysis from raw data, it can reject individual analyses of poorer quality because of their major oxide composition and the maximum acceptable errors.

All the parameters needed for calculating mean and intercept ages are computed and grouped in a specific table ready for plotting with the ISOPLOT program (Ludwig, 1999) to obtain statistics from suitable diagrams. The *EPMA Dating* program follows the method by Cocherie and Albarede (2001) for U–Th–Pb age calculation. It produces a "result table" giving: (1) the age and error from the slope of a Pb vs. Th* diagram (Cocherie et al., 1998); (2) the U–Th–Pb age at the centroid of the best fit line; (3) the Th–Pb age (intercept with Th / Pb axis) and the U–Pb age (intercept with U / Pb axis) from the Th / Pb vs. U / Pb diagram. All ages are given with absolute errors. All calculations are done at 2σ level.

The three starting assumptions behind EPMA U–Th–Pb dating of monazite are: (1) common Pb is negligible as compared to the amount of thorogenic and uranogenic lead; (2) no radiogenic Pb loss has occurred since system closure; (3) a single age is involved at the size level of each individual spot analysis. After comparison with conventional isotopic U–Pb age determinations, it is now accepted that EPMA resolution allows to avoid inclusions and altered domains that could potentially contain common Pb. Systematic BSE study was performed to investigate monazite microtexture for all mounted grains.

5. Monazite geochronology

5.1. Migmatite

5.1.1. Puylaurent migmatite — BE3

BSE images of monazite from Puylaurent migmatite show large monazite crystals (≥ 180 μm) with complex zoning that express variations in chemical composition (Fig. 4a, b). EPMA U–Th–Pb data on nine grains are presented in (Cocherie et al., 2005). These data are summarized in Table 1 and hereafter. All grains show significant variation in Th + U content (Table 1). Most grains exhibit patchy zoning (Fig. 4b) though Grain 12 shows concentric zoning (Fig. 4a). Due to the large range in Th / U ratio, i.e., 6.7 ± 7.5 (SD), the chemical composition of the monazite grains is favorable for using the Th / Pb vs. U / Pb diagram. Good data spread is obtained. The intercept ages are well defined and similar within error (U–Pb age: 313 ± 10 Ma and Th–Pb age: 333 ± 10 Ma). An isochron age of 323 ± 3 Ma is calculated at the centroid of the population, using analyses obtained on 8 grains. The more complicated Grain 12 shows two main domains on the BSE image (Fig. 4a). The bright rim of the grain has the same composition as the eight other monazites with a high U content and large Th / U variation (Table 1). Thirty-eight analyses gave a precise age at 324 ± 6 Ma using the Th / Pb vs. U / Pb diagram. As indicated by the BSE image, the core of this grain has a very distinct composition (Table 1), with a much lower U content of around 1000 ppm, and a large and rather constant Th / U ratio that is not favorable for using the Th / Pb vs. U / Pb diagram. For that reason we used the more suitable isochron plot (Pb vs. Th*) of Suzuki and Adachi, 1991a and Suzuki and Adachi, 1991b, which provides an isochron age of 550 ± 86 Ma plotting 34 analyses (Cocherie et al., 2005).

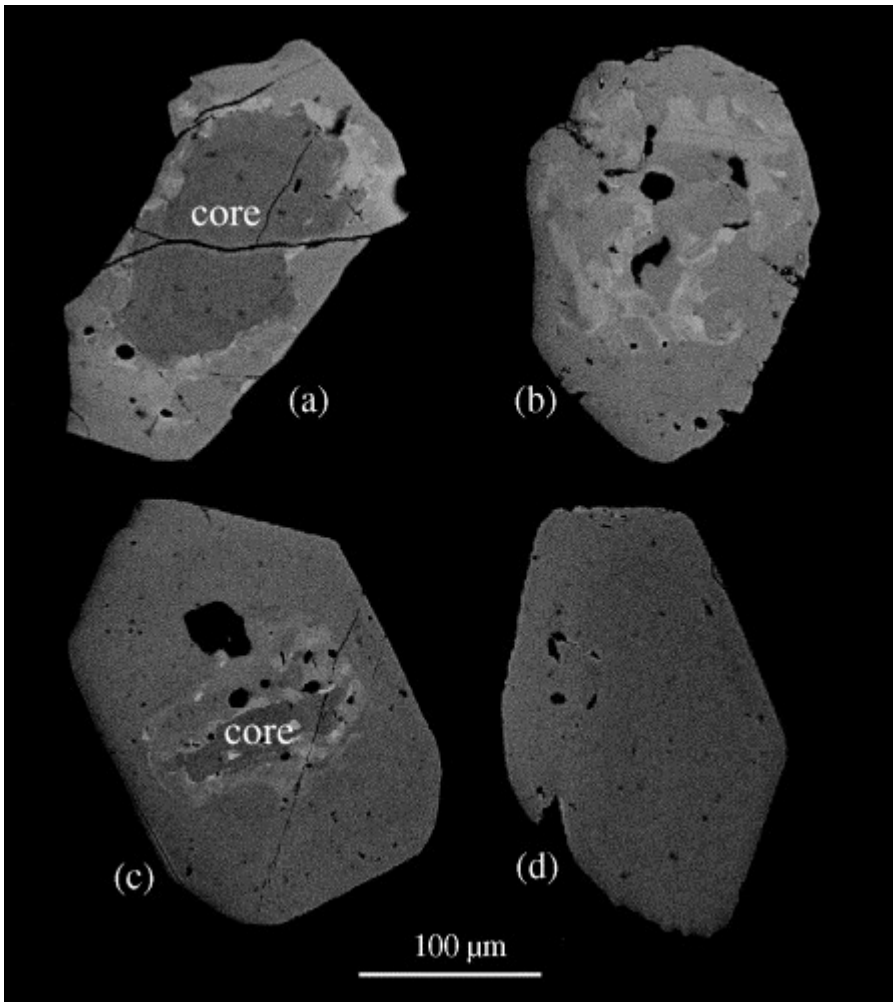

Fig. 4. Back-scattered electron (BSE) images of selected monazites from the Puylaurent migmatite: (a) sample BE3, Grain 12; (b) monazite with patchy zoning and inclusions from sample BE3, Grain 13; (c) and (d) sample BE13, Grain 3 and 10, respectively. (a) and (c) show euhedral monazites with inherited cores. Inherited cores are distinguishable from new overgrowths by their lower U contents. Ages show two generations of monazite. Monazite grains from migmatites contain numerous micro-inclusions of quartz, K-feldspar, biotite, zircon, apatite and allanite.

Despite the lower precision obtained on the core compared to the rim of the grain, a gap of about 200 Ma is clearly revealed. The rim of Grain 12 implies an episodic growth of monazite involving recrystallization or replacement of the original crystal. In addition, because the average age calculated on the rim is exactly the same as that calculated on the other grains that are homogeneous in age, it is demonstrated that no diffusion took place during this process.

5.1.2. Puylaurent migmatite — BE13

Back-scattered electron (BSE) images of monazites from BE13 migmatite again show large monazite crystals (≈180 μm), without zoning but locally containing small darker domains in the inner part of the grains (Fig. 4c and d). Seven grains were selected for electron microprobe

analysis, all showing limited variations in Th and U content (Table 1). A representative BSE image is shown in Fig. 4d. The Th / U ratio does not change drastically. Consequently, the data (6 out of 7 grains) do not widely spread in the Th / Pb vs. U / Pb diagram (Fig. 5a) leading to relatively large errors for the intercept ages (U–Pb age: 329 + 66/− 47 Ma and Th–Pb age: 315 + 50/− 70 Ma). An age of 322 ± 7 Ma can be calculated at the centroid (Fig. 5a). Grain 3 was carefully studied because it is representative of heterogeneous monazite extracted from the migmatite. The small darker core is significantly enriched in Th and depleted in U compared to the homogeneous grains or the rim of this grain. An unusually low number of analyses (8) was done on the core because of its small size. The data plot close to the Th / Pb axis (Fig. 5b). Despite the large error on the intercept ages (U–Pb age: 521 + 189/− 244 Ma and Th–Pb age: 550 + 75/− 59 Ma), it is clear that the analyses relate to a domain homogeneous in age and it is thus possible to calculate an age at the centroid of the population at 543 ± 25 Ma. A much larger number of data (n = 111) has been recorded from the outer part of Grain 3, providing a precise mean age at 329 ± 5 Ma despite clustering of the data (Fig. 5c). The two intercept ages are similar within analytical errors: 337 + 35/− 44 and 323 + 39/− 32 Ma for U–Pb and Th–Pb ages, respectively. The age obtained on the rim from Grain 3 is identical to that calculated at 322 ± 7 Ma on the six other grains. Due to the better statistic obtained on the rim of Grain 3, the age of 329 ± 5 Ma will be considered as the age of the migmatization event, equivalent to the age 323 ± 3 Ma derived from monazite from Puylaurent migmatite BE3. Again, we observe that limited and clearly defined domains of the grains are totally affected by recrystallization or replacement during the last recorded event, leaving the inner part of some grains unaffected by this last thermal event. To summarize, monazites of both migmatites yield an age between 329 ± 5 and 323 ± 3 Ma interpreted as the timing of migmatization, and they contain relic cores recording the age of their protolith at about 550–543 Ma. The experimental regression line calculated with the data is compared to the theoretical isochron. If both are close to each others, it is assumed that analytical data are related to a single chronological event.

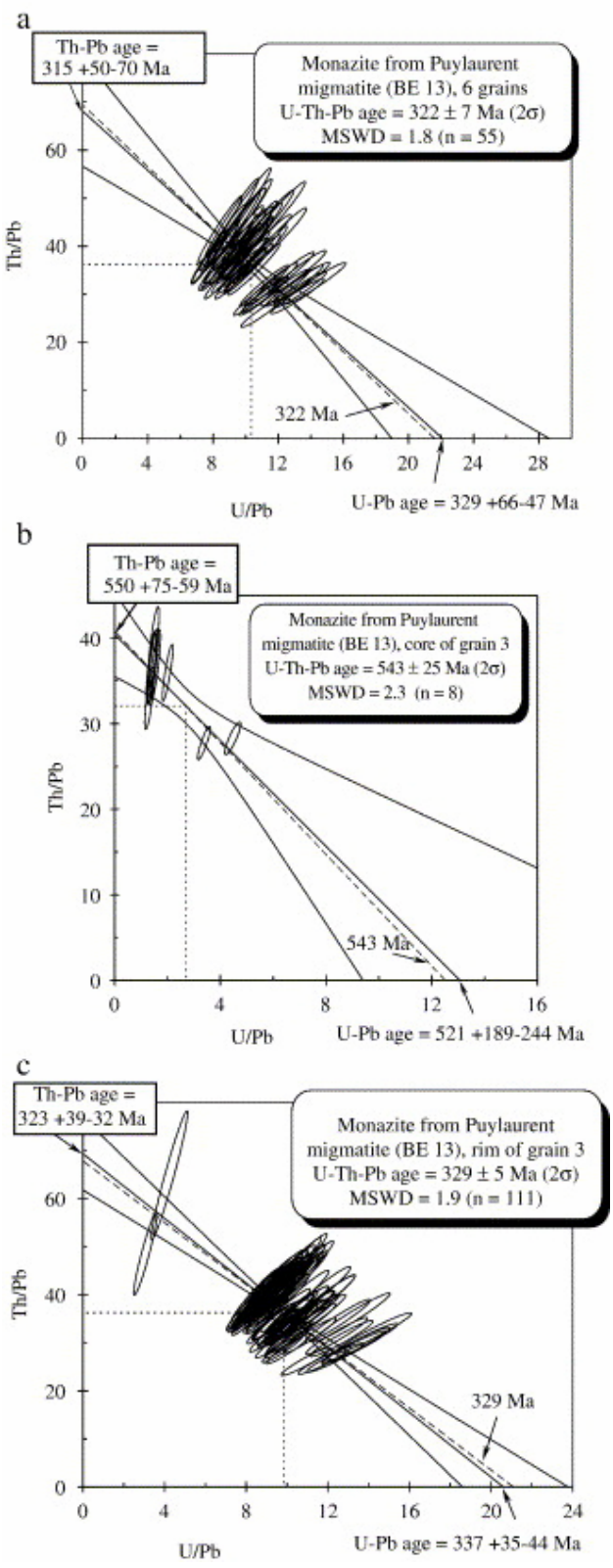

Fig. 5. U / Pb vs. Th / Pb isochron diagrams for monazite from analysed migmatites. All errors are quoted at 95% confidence level and error ellipses are plotted as 2σ. (a) Puylaurent (BE 13); (b) and (c) core and rim of Grain 3 from Puylaurent (BE 13). In Th / Pb vs. U / Pb diagram, the isochron age is calculated at the centroid of the population where error is least.

5.2. Granite

5.2.1. Rocles granite — sample Ro

In this rock, monazite is very rare and only four small grains (< 50 μm) were extracted. The total amount of U + Th remains rather constant around 10 wt.%, leading to poorly contrasted BSE images (Fig. 6a). By contrast, the Th / U ratio varies widely at 2.4 ± 2.2, making the Th / Pb vs. U / Pb diagram very efficient for calculating the mean age of the population. U seems to replace Th progressively in the monazite lattice during crystallization of the mineral. A precise mean age of 318 ± 3 Ma was calculated (Fig. 7a). The intercept ages are well defined at 321 ± 7 and 312 + 16/− 14 Ma for U–Pb and Th–Pb ages, respectively, nicely constraining the mean age.

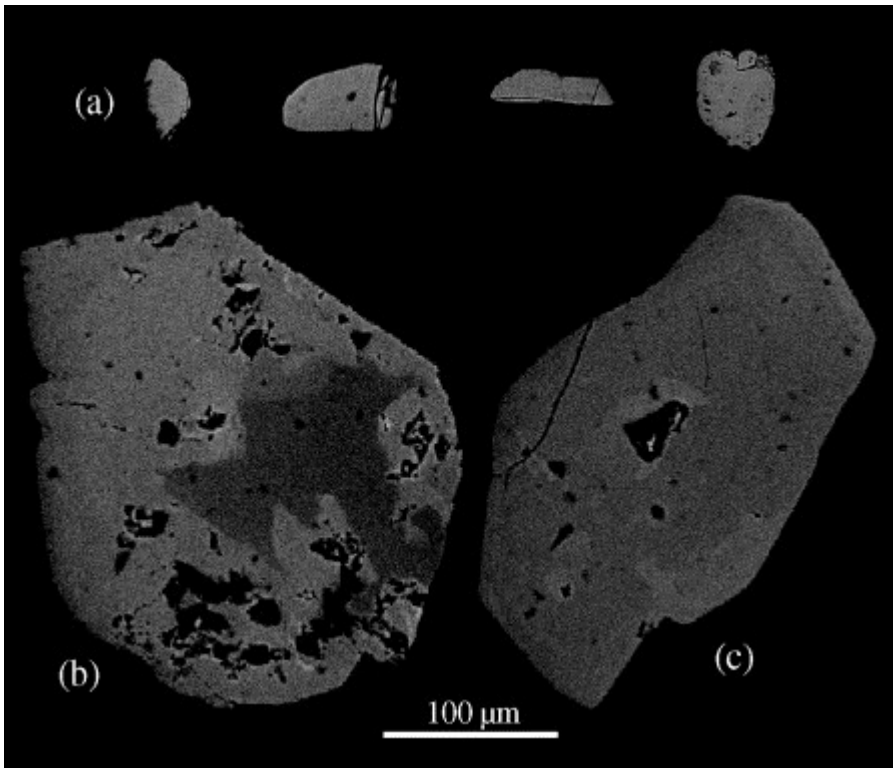

Fig. 6. BSE images of monazite grains from Rocles leucogranite and dykes. (a) Rocles granite: note common micro-inclusions and irregular grain boundaries related to alteration processes and mineral replacement, especially allanite, huttonite. (b) Leucogranite dykes, sample BE12, Grain 3. (c) Sample BE15: Grain 6.

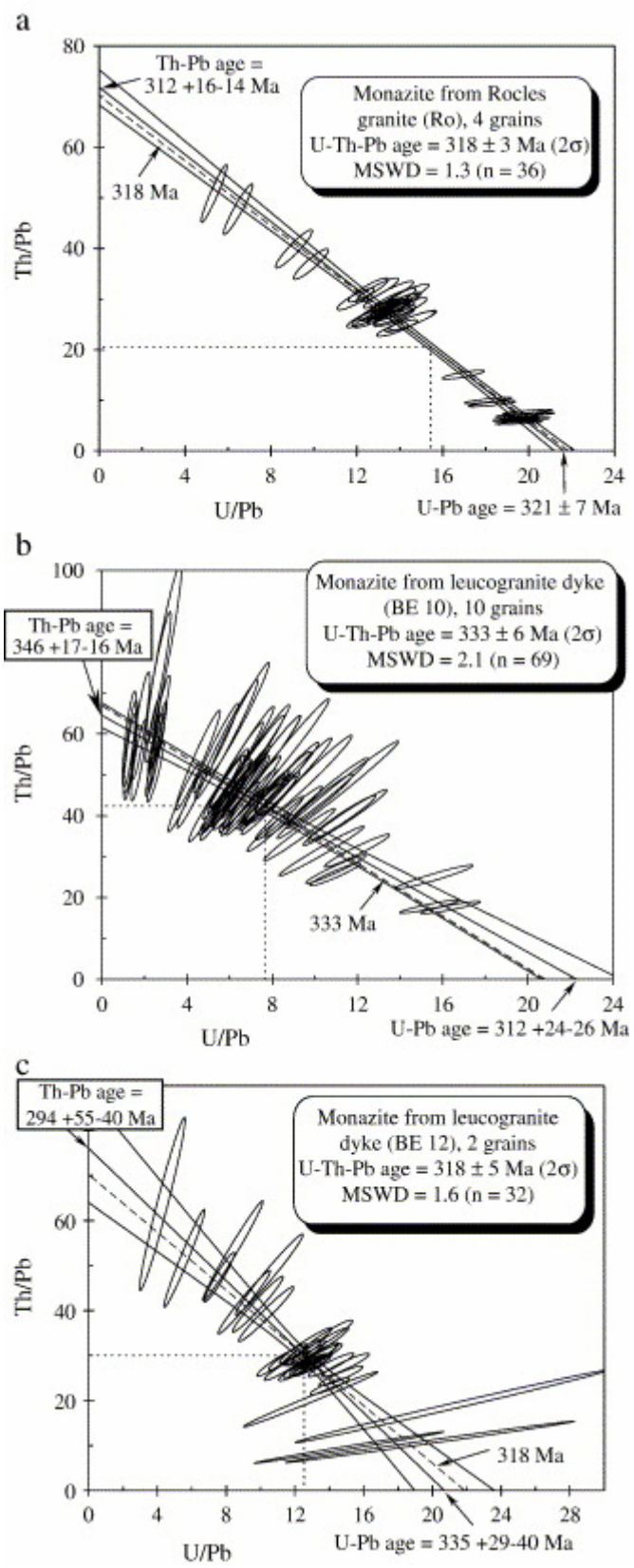

Fig. 7. U / Pb vs. Th / Pb isochron diagram for monazite from the granites. All errors are quoted at 95% confidence level and error ellipses are plotted as 2σ. (a) Rocles (Ro). (b) Leucogranite dyke (BE10). (c) Leucogranite dyke (BE12).

5.2.2. Leucogranite dyke — BE10

Ten monazite grains were extracted from the leucogranite dyke BE10. Th content remains nearly constant for all analysed domains at 5.2 ± 1.2 wt.%, while U content varies significantly at 0.8 ± 0.6 wt.% leading to considerable variation in Th / U ratio (Table 1). Consequently a large spread of data is observed in the Th / Pb vs. U / Pb diagram (Fig. 7b). The regression line is not strictly parallel to the reference isochron, but the two U–Pb and Th–Pb intercept ages of 312 + 24/− 26 and 346 + 17/−16 Ma are similar within errors. At the centroid of the population (n = 69), a mean age has been calculated at 333 ± 6 Ma.

5.2.3. Leucogranite dyke — BE12

Only two monazite grains were extracted from this granite dyke (BE12). As indicated by the zoning of one of the two grains (Fig. 6b) the grains are heterogeneous in composition. Furthermore, due to the large variation of U content (2.0 ± 1.0 wt.%), the Th / U ratio varies widely with the zoning. The intercept U–Pb and Th–Pb ages are similar within the errors, allowing us to calculate a mean age of 318 ± 5 Ma where the age is the most precisely defined at the centroid of the population (Fig. 7c).

5.2.4. Leucogranite dyke — BE15

Ten monazite grains were extracted from a third leucogranite dyke (sample BE15, Fig. 1). The results from this rock are reported in Cocherie et al. (2005) and summarized shortly hereafter. On a representative BSE image (Fig. 6c) no significant zoning is visible. Almost all individual data are characterized by a very high U content and a Th amount around 4 wt.% (excluding core of grain 5). This gives a high level of Pb despite the Variscan age of the rock and thus an unusually good precision of around ± 28 Ma can be derived for each individual spot. Furthermore, the variation in U content is significant at 4.0 ± 1.3 wt.% (Table 1). The mean age calculated from the data obtained on nine grains is 311 ± 5 Ma (Cocherie et al., 2005). One grain shows a very different core composition with much higher Th (14.1 ± 3.3 wt.%) and much lower U (0.4 ± 0.1 wt.%) contents, giving rise to high but constant Th / U ratio of 35 ± 5. This constant ratio is not suitable for using the Th / Pb vs. U / Pb diagram to calculate a mean age (Fig. 8a). In such a case, the most suitable isochron diagram is that of Suzuki and Adachi (1991a), because the $U + Th_{tot}$ content is very high and changes significantly. The well-defined slope gives a precise age at 341 ± 14 Ma associated with an intercept very close to the origin (Fig. 8b). The dark border of Grain 5 shows a composition quite similar to the nine other grains, giving a mean age of 309 ± 4 Ma at the centroid of the 43 spot analyses (Cocherie et al., 2005). Within the analytical error, this age is identical to that obtained on the nine other grains (311 ± 5 Ma). Consequently, the age of 341 ± 14 Ma is interpreted as a relic age while 311 ± 5 Ma is regarded as the recrystallization age of the monazite during emplacement of this granite dyke.

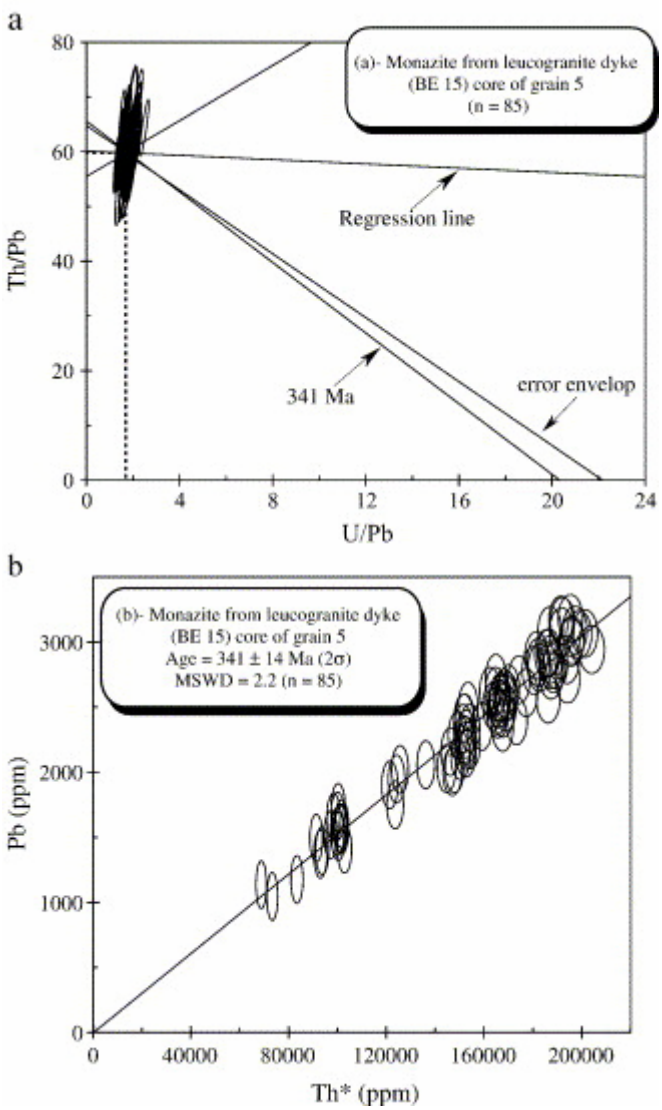

Fig. 8. Leucogranite dyke (BE 15). U / Pb vs. Th / Pb isochron diagram for monazite grain 5. As shown by the error envelop, the lack of spread of the data leads to a huge uncertainty on the slope of the regression line. Furthermore, the theoretical isochron is outside of the area defined by the error envelop. This diagram is not suitable for such data associated with constant Th / U ratio. Pb = *f*(Th*) isochron diagram allowing to calculate a rather precise age isochron at 341 ± 14 Ma with the same data, owing to the large variation in Th + U.

6. Discussion

Like zircon, inherited monazite cores or grains are common, indicating that a significant portion of crustal material is incompletely melted during genesis of granitoids. Such grains were identified in both migmatites (Puylaurent, BE3 and BE13) and leucogranite dykes (BE15). A high Th / U ratio (> 20) linked to a quite low U content (< 0.5 wt.%) characterizes all inherited monazite cores. This is of great importance for the bulk budget of trace elements such as Zr, Hf, Th and U, when modelling petrogenetic processes. The sharp boundary between core and rim observed on BSE images is also obvious on calculated ages giving evidence for a lack of significant Pb diffusion between the two domains.

A second type of compositional zoning in monazite is the very common patchy zoning (Fig. 4b). It has already been described by Bingen and van Breemen (1998), Zhu and O'Nions (1999), Foster et al. (2002) and Cocherie et al. (2005). Monazite from migmatite, leucocratic granite and granite dykes from this study exhibits such a zoning. It is related to high and variable U contents up to levels higher than Th (> 5 wt.%), leading to a large range in Th / U ratio. To generate such zoning, Zhu and O'Nions (1999) concluded of the need of complex processes such as "intergrowth of monazite crystals" or "episodic growth or regrowth involved by recrystallization or replacement of original crystals". In addition, they stressed the fact that the diffusion transport of the elements in monazite remains very low even at temperature of granulite facies metamorphism. The episodic processes that yield patchy zoning textures, appear to take place in a relatively short time span beyond resolution by the EMPA method (Cocherie et al., 2005).

Despite the lack of a clear understanding of the mechanisms governing monazite crystallization, the observed ages correspond to main geological events that have affected the Cévennes area. Post-thickening crustal melting responsible for Variscan magmatism and high-temperature regional metamorphism in the Cévennes area is geologically well documented (Duthou et al., 1984, Ledru et al., 1989, Pin and Duthou, 1990, Montel et al., 1992, Faure et al., 2001 and Faure et al., 2002).

EPMA dating of monazites in the migmatite suggests that, in the northern Cévennes, anatexis took place between 329 and 323 Ma. The crustal material reworked during crustal melting is dated at 550–543 Ma on both BE3 and BE13 migmatite samples. This protolith age agrees with previous results, since the augen orthogneiss west of the Velay Dome is dated at 528 ± 9 Ma by whole-rock Rb–Sr dating (R'kha Chaham et al., 1990). More generally, Early Cambrian orthogneisses are well known from the Massif Central (Duthou et al., 1984).

The monazite age of the Rocles leucogranite at 318 ± 3 Ma is significantly older than the previous Rb–Sr age of 302 ± 3 Ma (Caen-Vachette et al., 1981) which was calculated using whole rocks of various composition with very different $^{87}Rb / ^{86}Sr$ ratio (from 1.4 to 70) suggesting non-cogenetism of the related facies. Consequently, the age of the Rocles pluton given by monazite is more reliable than that given by the Rb–Sr whole rock method. The age of 318 ± 3 Ma is slightly younger than that of migmatization, but overlaps within age uncertainty. Thus, it can be argued that the leucogranite magmatism corresponds to a late stage of the same crustal melting event.

The leucogranite dykes (BE12 and BE15) were emplaced between 318 and 311 Ma, i.e., later than the migmatization but at the same time as, or immediately after, the Rocles granite. Conversely, the 333 ± 6 Ma age of the BE10 leucogranite dyke suggests that this vein was closely related to migmatization. Actually, the location of both the BE12 dyke and the Rocles granite along the Cévennes micaschist/gneiss contact and the similar deformation fabrics suggest that they belong to the same syn-tectonic event. Therefore, these dykes can be considered as differentiated products of the Rocles granite, emplaced during the same period in the same tectonic setting at the end of migmatization. Fig. 9 summarizes these results and shows that the migmatization stage took place before the leucogranite emplacement without any significant time gap.

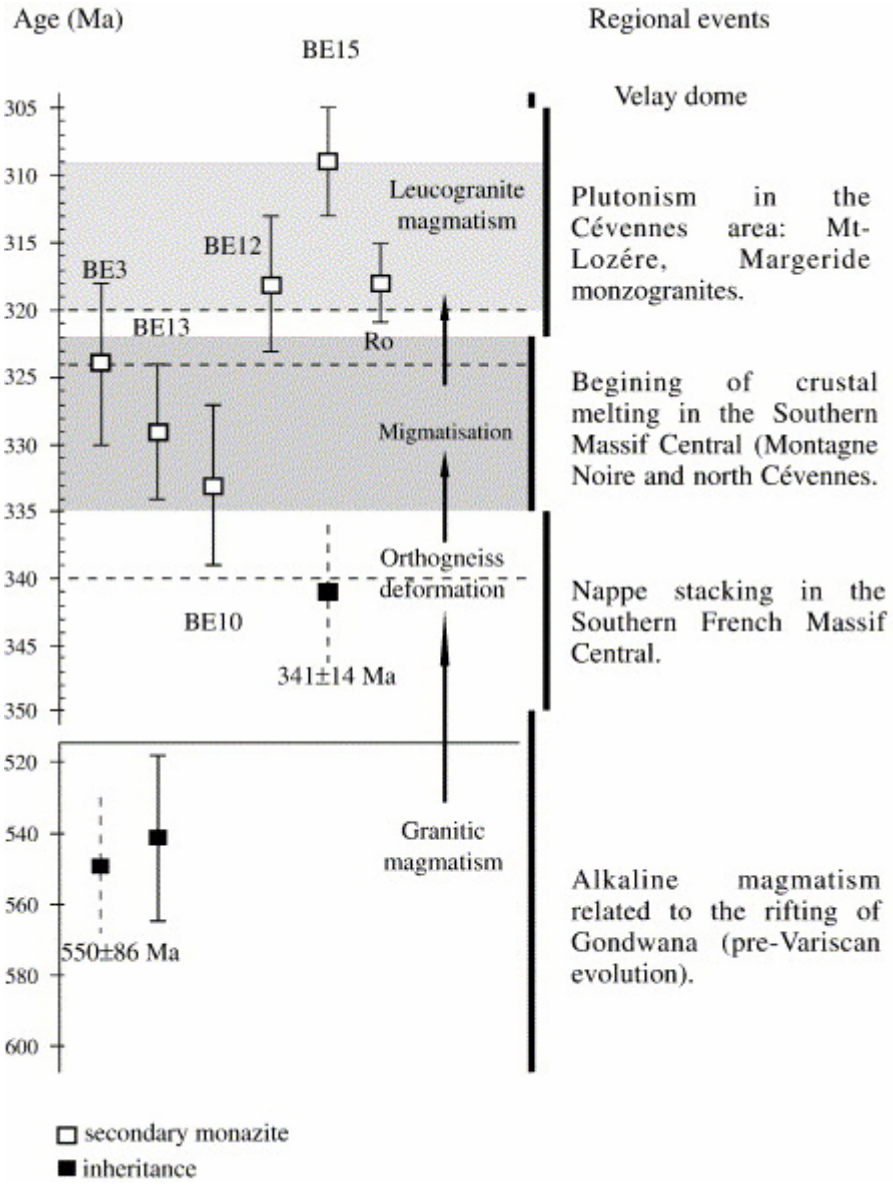

Fig. 9. Time scale with dated samples. In spite of overlapping error bars, two events can be distinguished: 329–323 Ma migmatization and 318–311 Ma leucogranite magmatism. The 550–543 Ma date is the age of the granite corresponding to the migmatite protolit

7. Conclusions

This paper provides a new example of the value of EPMA monazite geochronometry to distinguish crustal melting and metamorphic processes with age resolution of ± 5 Ma. Although mostly discussed for zircon, we show that inheritance and chemical changes are important phenomena in monazite as well, and that this mineral enables us to decipher polyphase tectonic–metamorphic events. Monazite composition reflects the chemical change within the source material from which monazite crystallized. The BSE images of zoned monazite grains show sharp variation in their chemical composition, which is well correlated with the age data. The measured in situ ages from rims of zoned monazites in the migmatites represent the time of peak metamorphism (migmatization) and monazite dissolution and

regrowth while inherited relic core can sometimes be preserved. On the other hand, commonly observed patchy zoning does not show any correlation with punctual ages.

When compiled with the available geochronology data of the French Massif Central, our measurements show a migmatitic event at about 329–323 Ma slightly before the already well known 318–311 Ma magmatic event, within a major crustal melting event taking place from 333 to 311 Ma. The latter Late Visean–Early Namurian thermal event, described from the northern part of Massif Central (e.g., Faure et al., 2002), remains poorly understood in the southern part. Forthcoming work will provide new data on the post-orogenic thermal processes in this part of the Variscan Belt.

Acknowledgements

The authors are grateful to P. Jezequel for mineral separation. Special thanks are due to C. Gilles, J. Breton and O. Rouer for their excellent EMPA and SEM work at BRGM. The authors wish also to thank B. Bingen, M. Erambert and U. Andersson who helped us to improve the manuscript. The work for this BRGM contribution (no. 2887) was supported financially by a BRGM research grant and the “Région Centre”.

References

Bingen and van Breemen, 1998 B. Bingen and O. van Breemen, U–Pb monazite ages in amphibolite- to granulite-facies orthogneiss reflect hydrous mineral breakdown reactions: Sveconorwegian Province of SW Norway, *Contributions to Mineralogy and Petrology* **132** (1998), pp. 336–353.

Braun et al., 1998 I. Braun, J.M. Montel and C. Nicollet, Electron microprobe dating of monazite from high-grade gneisses and pegmatites of the Kerala Khondalite Belt, southern India, *Chemical Geology* **146** (1998), pp. 65–85.

Caen-Vachette et al., 1981 M. Caen-Vachette, J.P. Couturié and A. Fernandez, Age westphalien du granite de Rocles (Cévennes, massif Central Français), *Comptes rendus de l'Académie des Sciences, Paris, II* **293** (1981), pp. 957–960.

Caron, 1994 Caron, C. 1994. Les minéralisations Pb–Zn associées au Paléozoïque inférieur d'Europe méridionale. Traçage isotopique Pb–Pb des gîtes de l'Iglesiente (SW Sardaigne) et des Cévennes et évolution du socle encaissant par la géochronologie U–Pb, ^{40}Ar–^{39}Ar et K–Ar. Ph.D. thesis, University of Montpellier II. 288 pp.

Cocherie and Albarede, 2001 A. Cocherie and F. Albarede, An improved U–Th–Pb age calculation for electron microprobe dating of monazite, *Geochimica et Cosmochimica Acta* **65** (2001), pp. 4509–4522.

Cocherie et al., 1998 A. Cocherie, O. Legendre, J.J. Peucat and A.N. Kouamelan, Geochronology of polygenetic monazites constrained by in situ electron microprobe Th–U–total Pb determination: implications for lead behaviour in monazite, *Geochimica et Cosmochimica Acta* **62** (1998), pp. 2475–2497

Cocherie et al., 2005 A. Cocherie, E. Be Mezeme, O. Legendre, C.M. Fanning, M. Faure and P. Rossi, Electron-microprobe dating as a tool for determining the closure of Th–U–Pb systems in migmatitic monazites, *American Mineralogist* **90** (2005), pp. 607–618.

Crowley and Ghent, 1999 J.L. Crowley and E.D. Ghent, An electron microprobe study of the U–Th–Pb systematics of metamorphosed monazite: the role of Pb diffusion versus overgrowth and recrystallization, *Chemical Geology* **157** (1999), pp. 285–302.

Duthou et al., 1984 J.L. Duthou, J.M. Cantagrel, J. Didier and Y. Vialette, Paleozoic granitoids from the French Massif Central: age and origin studied by ^{87}Rb / ^{87}Sr system, *Physics of the Earth and Planetary Interiors* **35** (1984), pp. 131–144

Faure et al., 1997 M. Faure, C. Leloix and J.Y. Roig, L'évolution polycyclique de la chaîne hercynienne, *Bulletin de la Société Géologique de France* **168** (1997) (6), pp. 3–14.

Faure et al., 2001 M. Faure, X. Charonnat, A. Chauvet and Y. Chen, Tectonic evolution of the Cévennes para-autochthonous domain of the Hercynian French Massif Central and its bearing on ore deposits formation, *Bulletin de la Société Géologique de France* **172** (2001), pp. 687–696.

Faure et al., 2002 M. Faure, P. Monié, H. Maluski, C. Pin and C. Leloix, Late Visean thermal event in the northern part of the French Massif Central. New ^{40}Ar / ^{39}Ar and Rb–Sr isotopic constraints on the Hercynian syn-orogenic extension, *International Journal of Earth Sciences* **91** (2002), pp. 53–75.

Foster et al., 2002 G. Foster, H.D. Gibson, R. Parrish, M. Horstwood, J. Fraser and A. Tindle, Textural, chemical and isotopic insights into the nature and behaviour of metamorphic monazite, *Chemical Geology* **191** (2002), pp. 183–207.

Isnard, 1996 Isnard, H. 1996. Datation par la méthode U / Pb sur monazites des granites du Mont-Lozère et de l'Est de la Margeride. DEA (unpublished Master thesis) University of Montpellier. 50 pp.

Ledru et al., 1989 P. Ledru, J.M. Lardeaux, D. Santallier, A. Autran, J.M. Quenardel, J.P. Floc'h, G. Lerouge, N. Maillet and A. Ploquin, Où sont les nappes dans le Massif Central Français?, *Bulletin de la Société Géologique de France* **8, V** (1989) (3), pp. 605–618.

Ludwig, 1999 Ludwig, K.R., 1999. Users manual for ISOPLOT/EX, version 2. A geochronological toolkit for Microsoft Excel. Berkeley Geochronology Center, Special Publication 1a.

Mialhe, 1980 Mialhe, J., 1980. Le massif granitique de la Borne (Cévennes), étude pétrographique, géochimique, géochronologique et structurale. Ph.D. thesis, University of Clermond-Ferrand.

Montel et al., 1992 J.M. Montel, C. Marignac, P. Barbey and M. Pichavant, Thermobarometry and granite gneiss: the Hercynian low-*P*, high-*T* Velay anatectic dome (French Massif Central), *Journal of Metamorphic Geology* **10** (1992), pp. 1–15.

Palm, 1957 Palm, Q.A., 1957. Les roches cristallines des Cévennes médianes, à hauteur de Largentière, Ardèche, France. Ph.D. thesis, University of Utrecht, Geologia Ultraiectina, vol. 3. 121 pp.

Parrish, 1990 R.R. Parrish, U–Pb dating of monazite and its application to geological problems, *Canadian Journal of Earth Sciences* **27** (1990), pp. 1431–1450.

Pin and Duthou, 1990 C. Pin and J.L. Duthou, Sources of Hercynian granitoids from the French Massif Central: inferences from Nd isotopes and consequences for crustal evolution, *Chemical Geology* **83** (1990), pp. 281–296.

Pommier et al., 2002 A. Pommier, A. Cocherie and O. Legendre, EPMA Dating User's Manual: Age Calculation from Electron Probe Microanalyser Measurements of U–Th–Pb. BRGM Documents (2002) 9 pp..

R'kha Chaham et al., 1990 K. R'kha Chaham, J.P. Couturié, J.L. Duthou, A. Fernandez and G. Vitel, L'orthogneiss oeillé de l'Arc de Fix: un nouveau témoin d'âge cambrien d'un magmatisme hyper alumineux dans le Massif Central Français, *Comptes rendus de l'Académie des Sciences, Paris* **311** (1990), pp. 845–850.

Suzuki and Adachi, 1991a K. Suzuki and M. Adachi, Precambrian provenance and Silurian metamorphism of the Tsubonosawa paragneiss in the south Kitakami terrane, northeast Japan, revealed by the chemical Th–U–total Pb isochrone ages of monazite, zircon and xenotime, *Geochemical Journal* **25** (1991), pp. 357–376. Abstract-GEOBASE

Suzuki and Adachi, 1991b K. Suzuki and M. Adachi, The chemical Th–U–total Pb isochron ages of zircon and monazite from the gray granite of the Hida Terrane, Japan, *Journal of Earth Sciences, Nagoya University* **38** (1991), pp. 11–37.

Townsend et al., 2000 K.J. Townsend, C.F. Miller, J.L. D'Andrea, J.C. Ayers, T.M. Harrison and C.D. Coath, Low temperature replacement of monazite in the Ireteba granite, southern Nevada: geochronological implications, *Chemical Geology* **172** (2000), pp. 95–112.

Weisbrod, 1968 A. Weisbrod, Les conditions du metamorphisme dans les Cévennes médianes, *Comptes rendus de l'Académie des Sciences, Paris* **266** (1968), p. 775.

Williams and Jercinovic, 2002 M.L. Williams and M.J. Jercinovic, Microprobe monazite geochronology: putting absolute time into microstructural analysis, *Journal of Structural Geology* **24** (2002), pp. 1013–1028.

Zhu and O'Nions, 1999 X.K. Zhu and O'Nions, Zonation of monazite in metamorphic rocks and its implications for high temperature thermochronology: a case study from the Lewisian terrain, *Earth and Planetary Science Letters* **171** (1999), pp. 209–220.